第51卷第6期 中国科学技术大学学报 Vol. 51, No. 6
2021年6月 JOURNAL OF UNIVERSITY OF SCIENCE AND TECHNOLOGY OF CHINA Jun. 2021
Received: 2021-05-09; Revised: 2021-06-17 doi:10.52396/JUST-2021-0128

A new high-resolution $\delta^{13}C_{carb}$ record for the Early-Middle Triassic: Insights from the Tianshengqiao section, South China

ZHANG Guijie[1*], ZHANG Xiaolin[1], ZHOU Changyong[2], HUANG Jinyuan[2], ZHANG Qiyue[2], HU Shixue[2], WEN Wen[2], HUANG Xiemin[1]
1. School of Earth and Space Sciences, University of Science and Technology of China, Hefei 230026, China;
2. Chengdu Center, China Geological Survey, Chengdu 610081, China
* Corresponding author. E-mail: zhanggj@ustc.edu.cn

Abstract: Previous studies have documented remarkable changes in the carbon cycle during the Early Triassic. To verify these trends and improve our understanding of carbon cycling during the Early-Middle Triassic, we investigate the new $\delta^{13}C_{carb}$ record for the Early-Middle Triassic in the Tianshengqiao section of South China. Our study shows that the $\delta^{13}C_{carb}$ values in the Tianshengqiao section have received minimal diagenetic alterations. The $\delta^{13}C_{carb}$ profile initially shows a negative excursion of 2.2‰ within the Member I of the Jialingjiang Formation, followed by a positive excursion of 3.8‰ in the lower part of the Member III of the Jialingjiang Formation. After that, $\delta^{13}C_{carb}$ displays a negative excursion of 2.5‰ in the Member III of the Jialingjiang Formation, followed by a positive excursion with a maximum of +5.0‰ at the base of the Member I of the Guanling Formation. Above the maximum value, the $\delta^{13}C_{carb}$ profile exhibits a third negative excursion and then recovers and stabilizes around +1‰ to +2‰ through the Member II of the Guanling Formation to the Yangliujing Formation. The observed trend of the $\delta^{13}C_{carb}$ profile in the Tianshengqiao section can be correlated with the global C-isotopic excursions derived from the coeval sections worldwide. The similarity of the Early-Middle Triassic $\delta^{13}C_{carb}$ profile to those from other sections worldwide is indicative of the near completeness of the stratigraphic interval of the Tianshengqiao section. Our results suggest that the $\delta^{13}C_{carb}$ profile in the Tianshengqiao section represents a global carbon cycle perturbation. The stratigraphic coincidence between the carbon cycle perturbation and the limited biotic recovery has been documented in the Tianshengqiao section, suggesting that the physical mechanism of the carbon cycle perturbation may have contributed to the prolonged biotic recovery.

Keywords: chemostratigraphic correlation; carbon cycle perturbation; prolonged biotic recovery; Early-Middle Triassic
CLC number: P593 **Document code**: A

1 Introduction

The end-Permian mass extinction represents the most devastating biotic crisis of the Phanerozoic, resulting in the loss of > 80% of marine species on a global scale[1,2]. The subsequent biotic recovery was prolonged for nearly 4−8 million years until the beginning of the Middle Triassic[3]. The combinations of geochemical, sedimentological and paleontological studies show that the Early Triassic is characterized by harsh environmental conditions, including global warming[4], widespread development of oceanic anoxia[5−8], and intensified weathering[9,10]. The most substantial evidence for environmental disturbance during the Early Triassic is a series of large fluctuations in C-isotope, suggesting that significant perturbation of the global carbon cycle occurred during this time[11−15]. However, the physical mechanism of the carbon cycle disturbance and its potential relationship to the prolonged biotic recovery remain poorly understood.

The detailed understanding of the Early-Middle Triassic carbon cycling requires additional high-resolution studies at various paleogeographic settings. Here we report a new high-resolution $\delta^{13}C_{carb}$ record from the Early-Middle Triassic successions in the Tianshengqiao section in Shizong, Yunnan, South

Citation: ZHANG Guijie, ZHANG Xiaolin, ZHOU Changyong, et al. A new high-resolution $\delta^{13}C_{carb}$ record for the Early-Middle Triassic: Insights from the Tianshengqiao section, South China. J. Univ. Sci. Tech. China, 2021, 51(6): 459−467.

China. The Tianshengqiao section preserves the continuous marine successions with a stratigraphic thickness of ~1000 m from the Early Triassic to the Middle Triassic, allowing us to establish a high-resolution $\delta^{13}C_{carb}$ profile. As a newly recognized outcrop, the biostratigraphic control in the Tianshengqiao section is relatively coarse. The C-isotopic chemostratigraphy can check the precise horizon of the critical stratigraphic boundary. Our data can provide new insights into the temporal evolution of carbon cycling and its possible link with the delayed biotic recovery.

2 Geological setting and stratigraphy

During the Early-Middle Triassic, the South China Block was situated in the eastern part of the Paleotethys Ocean. The Lower-Middle Triassic marine stratigraphic successions in South China are composed of various sedimentary facies. Five sedimentary provinces have been established for the Early Triassic marine sequences of South China, including the Lower Yangtze, Upper Yangtze, Youjiang, Cathaysia and Lijiang sedimentary provinces[16]. Of these, the Upper Yangtze sedimentary province preserves one of the most complete and best-studied Lower-Middle Triassic successions[16].

The Tianshengqiao section is located in Tianshengqiao village, approximately 20 km west of the Shizong town in Eastern Yunnan, South China. Tectonically, the Tianshengqiao section was situated in a shallow marine setting in the Upper Yangtze sedimentary province. The Lower-Middle Triassic successions in the Tianshengqiao section consist of the Jialingjiang, Guanling, and Yangliujing Formations in ascending order (Figure 1). The Jialingjiang Formation is subdivided into three members. The Member I primarily comprises the thin to medium bedded gray vermicular limestone containing gastropods and bivalves. The Member II is primarily composed of siltstone containing gastropods, bivalves, and plant debris fossils. The Member III is dominated by the thin to medium bedded vermicular limestone in the lower and middle parts and muddy limestone in the uppermost part. The Member III contains gastropods, bivalves, ammonoids, and crinoids. The occurrences of the ammonoids *Tirolites spinosus* and *Meekoceras* sp., the bivalve *Entolium discites microtis*, and the conodont *Neospathodus triangularis* in the Jialingjiang Formation indicate the Olenekian age[17,18]. Moreover, the conodonts assigned to the *Pachycladina-Parachirognathus* assemblage occurred in the uppermost

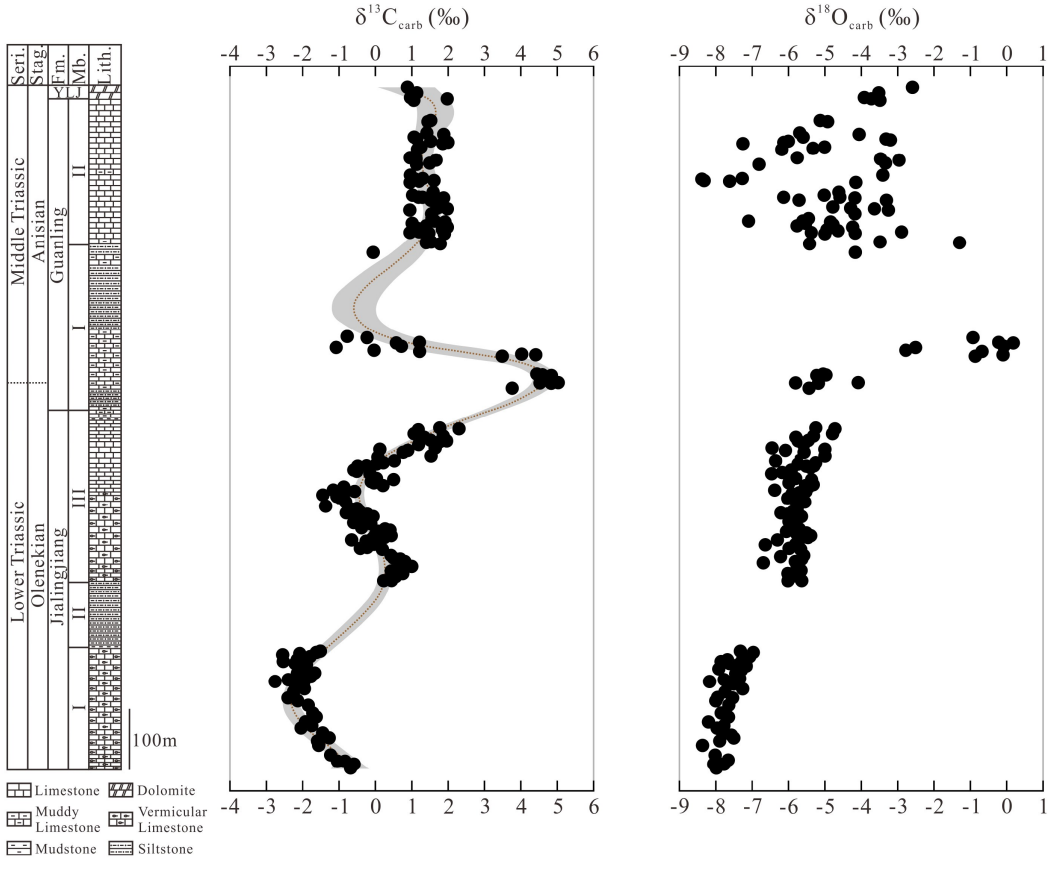

Figure 1. Lithostratigraphy and chemostratigraphy of $\delta^{13}C_{carb}$ and $\delta^{18}O_{carb}$ in the Tianshengqiao section. The brown dashed line and grey intervals on the isotopic data represent the polynomial fit and confidence interval, respectively. Abbreviations: YLJ = Yangliujing.

of the Member I of the Jialingjiang Formation, indicating deposition in the late Smithian[18].

The overlying Guanling Formation consists of two members. The Member I is primarily composed of muddy limestone interbedded with siltstone. This member contains gastropods, bivalves, crinoids, ammonoids, and plant debris fossils. The Member II is typified by limestone interbedded with muddy limestone. This member contains gastropods, bivalves, crinoids, and plant debris fossils. The occurrences of the bivalve *Costatoria goldfussi* and the conodont *Nicoraella kockeli* in the Guanling Formation indicate the Anisian age[19,20]. The Yangliujing Formation is dominated by dolostone.

3 Methods

Fresh rock samples were trimmed to remove weathered surfaces and visible veins, and then were cut into small pieces. Subsequently, the rock chips were individually powdered (<200 mesh) to avoid contamination. The analyses of $\delta^{13}C_{carb}$ and $\delta^{18}O_{carb}$ were performed at the China University of Geosciences in Wuhan. The powder samples (ca. 150 μg) were reacted with 102%–105% anhydrous phosphoric acid at 70℃ under vacuum in a Kiel IV carbonate device to liberate CO_2. The generated CO_2 was cryogenically purified and then automatically introduced into a MAT 253 Mass Spectrometer for $\delta^{13}C_{carb}$ and $\delta^{18}O_{carb}$ measurements. All the isotopic data are reported in units of per mille (‰) relative to the Vienna Peedee belemnite (VPDB) standard. Precision and calibration of the data were monitored by replicate analyses of a Chinese national standard GBW04416. The analytical precision was better than ±0.1‰ for $\delta^{13}C_{carb}$ and $\delta^{18}O_{carb}$.

4 Results

The samples from the Member I of the Jialingjiang Formation to the Yangliujing Formation were analyzed, except for the samples from the Member II of the Jialingjiang Formation, which are dominated by clastic rocks. Overall, the $\delta^{13}C_{carb}$ values in the Tianshengqiao section range from −2.8‰ to +5.0‰ (Table 1). The $\delta^{13}C_{carb}$ values initially display a negative excursion from −0.6‰ to −2.8‰ within the Member I of the Jialingjiang Formation, followed by a rise to +1‰ in the lower part of the Member III of the Jialingjiang Formation (Figure 1). The $\delta^{13}C_{carb}$ values show a second negative excursion from +1.0‰ to −1.5‰, followed by an increase to a maximum value of +5.0‰ at the base of the Member I of the Guanling Formation (Figure 1). Above the maximum value, the $\delta^{13}C_{carb}$ values display a third negative excursion and then recover and stabilize around +1‰ to +2‰ through the Member II of the Guanling Formation to the Yangliujing Formation (Figure 1).

5 Discussion

5.1 Evaluation of diagenetic influences

The primary C-isotopic signatures of carbonate sediments can be potentially influenced by diagenetic processes[21–26]. In order to discuss the stratigraphic and paleoenvironmental significance of the data, it is critical to evaluate the diagenetic effects on the primary isotopic signatures. The $\delta^{18}O$ values of carbonate sediments are vulnerable to diagenetic modifications due to a large reservoir of oxygen within the diagenetic fluids and the susceptibility of $\delta^{18}O$ values to diagenetic temperature[21]. It has been suggested that $\delta^{18}O_{carb}$ values lower than −10‰ may indicate significant diagenetic modifications[21]. In the present case, the $\delta^{18}O_{carb}$ values in the Tianshengqiao section range from −8.4‰ to +0.2‰, excluding the possibility of signi ficant diagenetic alterations (Figure 2).

Generally, the $\delta^{13}C_{carb}$ values are less susceptible to diagenetic alterations because most diagenetic fluids contain much lower carbon content compared to carbonate sediments. However, under the influence of diagenetic fluids which are enriched in organically derived carbon, both $\delta^{13}C_{carb}$ and $\delta^{18}O_{carb}$ are likely to be altered[22,23]. Therefore, the positive covariation of $\delta^{13}C_{carb}$ and $\delta^{18}O_{carb}$ is often used to identify diagenetic modifications in carbonate sediments[22,23]. A lack of significant positive correlation of $\delta^{13}C_{carb}$ and $\delta^{18}O_{carb}$ either for the individual intervals or the whole samples provides further evidence of minimal diagenetic modifications of the primary C-isotopic signatures (Figure 2).

5.2 Chemostratigraphic correlation with global trends

The Tianshengqiao section is constrained by the biozones of conodonts, as well as ammonoids and bivalves. The placement of the Olenekian stage is constrained by the occurrences of the ammonoids *Tirolites spinosus* and *Meekoceras* sp., the bivalve *Entolium discites microtis*, and the conodont *Neospathodus triangularis* in the Jialingjiang Formation[17,18]. Moreover, the placement of the upper Smithian is constrained by the occurrences of the conodonts assigned to the *Pachycladina-Parachirognathus* assemblage in the uppermost of the Member I of the Jialingjiang Formation[18]. The placement of the Anisian stage is constrained by the occurrences of the bivalve *Costatoria goldfussi* and the conodont *Nicoraella kockeli* in the Guanling Formation[19,20]. Within the biostratigraphic framework, the $\delta^{13}C_{carb}$ profile in the Tianshengqiao section can be correlated with those in the cotemporaneous sections globally[11–15].

Table 1. Geochemical data from the Tianshengqiao section.

Depth (m)	$\delta^{13}C_{carb}$ (‰)	$\delta^{18}O_{carb}$ (‰)	Depth (m)	$\delta^{13}C_{carb}$ (‰)	$\delta^{18}O_{carb}$ (‰)	Depth (m)	$\delta^{13}C_{carb}$ (‰)	$\delta^{18}O_{carb}$ (‰)	Depth (m)	$\delta^{13}C_{carb}$ (‰)	$\delta^{18}O_{carb}$ (‰)
1469.2	0.88	−2.59	1214.6	1.40	−1.30	806.7	−0.58	−5.52	672.1	0.75	−6.02
1460.2	1.14	−3.52	1212.6	1.78	−5.42	804.7	−1.46	−5.70	669.3	0.62	−5.89
1452.4	0.97	−3.92	1198.6	−0.06	−4.16	802.7	−0.87	−5.90	668.1	0.51	−5.86
1450.4	1.98	−3.72	1060.7	−0.78	−0.92	800.7	−1.45	−5.96	667.1	0.56	−5.64
1448.0	1.05	−3.48	1058.7	−0.23	−0.93	799.0	−1.06	−5.80	664.4	0.42	−5.76
1415.1	1.52	−5.13	1050.8	1.21	−0.22	798.2	−1.07	−5.85	662.4	0.45	−5.92
1413.1	1.44	−4.92	1049.8	0.57	0.18	795.3	−0.96	−6.02	660.6	0.45	−5.64
1394.8	1.41	−5.69	1044.4	0.72	−0.08	793.3	−0.82	−5.96	660.4	0.23	−6.01
1392.3	1.88	−4.06	1042.4	−1.08	−2.51	791.8	−0.91	−5.82	544.7	−1.52	−7.32
1387.8	1.06	−5.60	1037.9	−0.04	−2.77	789.3	−0.82	−5.55	542.7	−1.62	−6.97
1384.7	1.14	−3.32	1035.9	1.22	−0.68	782.4	−1.37	−5.76	540.7	−2.08	−7.00
1383.1	2.03	−3.20	1031.4	4.03	−0.10	780.4	−0.64	−5.82	538.7	−2.55	−7.29
1381.1	1.52	−6.00	1030.4	4.41	−0.10	778.4	−0.51	−5.78	535.7	−1.79	−7.06
1379.1	2.00	−6.13	1028.2	3.49	−0.86	777.4	−0.66	−5.76	532.7	−2.02	−7.25
1377.1	1.85	−7.25	999.1	4.44	−5.05	773.4	−0.43	−5.88	530.7	−2.15	−7.68
1371.5	1.25	−5.01	997.7	4.59	−4.97	771.4	−0.80	−6.21	527.9	−2.49	−7.74
1369.5	1.14	−5.32	996.7	4.84	−5.22	769.4	−0.22	−6.02	527.7	−2.53	−7.86
1367.5	1.16	−6.19	985.1	5.03	−4.08	767.4	−0.48	−5.93	524.8	−1.92	−7.33
1353.9	0.95	−5.76	984.6	4.52	−5.80	765.4	−0.07	−5.64	524.5	−2.21	−7.62
1351.9	1.12	−3.47	984.1	4.84	−5.18	763.2	−0.50	−5.67	522.5	−1.90	−7.24
1349.9	1.67	−2.96	976.0	3.76	−5.43	761.2	−0.15	−5.83	520.5	−1.91	−7.16
1344.9	1.49	−3.33	910.6	1.77	−5.25	759.2	−0.30	−5.84	517.5	−2.09	−7.34
1342.9	1.13	−6.81	909.1	2.30	−4.72	757.2	−0.37	−5.98	515.5	−2.11	−7.92
1325.2	0.96	−3.41	907.6	1.18	−4.74	755.2	−0.60	−5.81	513.5	−1.96	−7.30
1319.7	1.30	−7.27	901.0	1.06	−4.79	753.2	−0.13	−5.87	508.7	−1.67	−7.41
1318.7	1.09	−8.38	897.2	1.86	−5.31	746.9	−0.38	−5.79	508.5	−2.15	−7.48
1316.2	1.61	−8.32	895.2	1.34	−5.80	744.9	0.26	−5.71	507.8	−1.86	−7.45
1315.2	1.20	−7.62	890.2	1.52	−5.45	742.9	0.41	−5.90	505.8	−2.01	−7.46
1313.2	0.95	−4.15	889.2	1.96	−5.74	740.9	0.08	−6.06	502.8	−1.77	−7.46
1297.2	1.59	−4.61	887.7	1.77	−5.55	738.4	0.31	−5.51	499.8	−1.93	−7.34
1292.4	1.02	−5.02	883.2	1.19	−5.58	736.9	0.16	−5.71	497.8	−2.40	−7.77
1289.1	1.18	−4.59	877.6	1.64	−6.45	735.9	0.01	−5.76	494.8	−2.76	−8.17
1288.9	1.29	−6.13	875.6	0.12	−5.00	733.9	0.43	−5.39	492.8	−1.97	−7.61
1287.9	1.87	−4.17	873.6	0.89	−6.08	732.9	0.35	−5.57	490.8	−2.21	−7.51
1284.3	1.64	−5.71	870.6	0.76	−5.57	730.9	0.24	−5.47	482.8	−1.95	−7.26
1284.1	1.53	−3.31	864.6	1.53	−5.00	728.9	−0.09	−5.70	477.8	−2.25	−7.74
1273.2	1.77	−4.78	862.6	0.07	−5.72	726.9	−0.66	−6.31	468.8	−2.42	−7.95
1271.2	1.69	−4.29	856.6	0.52	−6.36	724.9	−0.26	−5.73	467.8	−2.41	−7.54
1270.2	1.98	−3.64	853.6	0.21	−5.25	721.9	−0.13	−5.72	463.0	−2.14	−8.00
1268.2	0.94	−3.25	851.6	0.03	−5.74	719.9	−0.04	−5.80	455.9	−1.85	−7.64
1262.0	1.55	−4.17	848.6	−0.24	−5.30	718.9	−0.33	−6.64	443.0	−1.72	−7.85
1254.3	1.55	−5.45	848.1	−0.49	−5.51	714.6	−0.23	−5.72	436.5	−1.63	−7.65
1250.3	1.71	−5.61	845.7	−0.44	−5.40	713.2	−0.42	−5.98	428.5	−1.93	−8.20
1250.1	1.63	−7.10	843.7	−0.17	−5.41	711.6	0.19	−5.67	422.5	−1.75	−7.78
1248.7	1.91	−4.84	841.7	−0.60	−5.92	701.7	0.43	−5.58	418.5	−2.05	−7.96
1246.4	1.01	−5.53	839.7	−0.51	−6.22	699.7	0.48	−6.22	410.5	−1.45	−7.81
1244.4	1.88	−4.78	837.7	−0.17	−6.17	697.7	0.49	−5.69	407.0	−1.32	−7.57
1242.4	1.39	−5.76	835.7	−0.15	−6.46	695.7	0.68	−5.64	402.4	−1.27	−7.50
1240.2	1.98	−4.23	831.7	−0.02	−5.98	691.7	0.81	−5.81	397.4	−1.59	−7.89
1238.3	1.15	−5.73	828.0	0.03	−5.80	689.7	0.66	−6.69	390.2	−1.56	−8.36
1236.1	1.84	−4.94	826.0	0.50	−5.37	687.7	0.96	−5.73	374.3	−1.24	−8.02
1234.2	1.31	−4.64	822.8	−0.11	−5.34	685.7	0.78	−5.74	366.1	−1.08	−7.65
1232.2	1.20	−2.89	820.8	−0.04	−5.98	683.7	1.00	−5.76	364.3	−1.05	−8.04
1231.2	0.95	−5.37	817.8	0.23	−5.32	680.2	0.78	−5.66	364.1	−0.84	−7.99
1230.2	1.47	−4.17	816.3	0.21	−5.53	679.1	0.72	−5.69	359.5	−0.60	−8.05
1229.1	1.90	−5.00	813.8	−0.87	−5.44	677.1	0.68	−5.66	359.3	−0.59	−7.77
1215.7	1.53	−3.48	808.8	−1.16	−6.38	676.1	0.43	−6.02	352.9	−0.68	−7.98

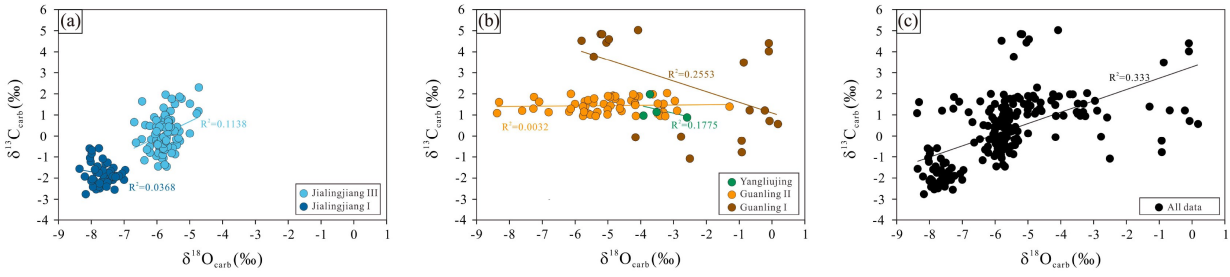

Figure 2. Cross-plot of $\delta^{13}C_{carb}$ and $\delta^{18}O_{carb}$ for the Jialingjiang Formation (a); cross-plot of $\delta^{13}C_{carb}$ and $\delta^{18}O_{carb}$ for the Guanling and Yangliujing Formations (b); cross-plot of $\delta^{13}C_{carb}$ and $\delta^{18}O_{carb}$ for all the samples (c).

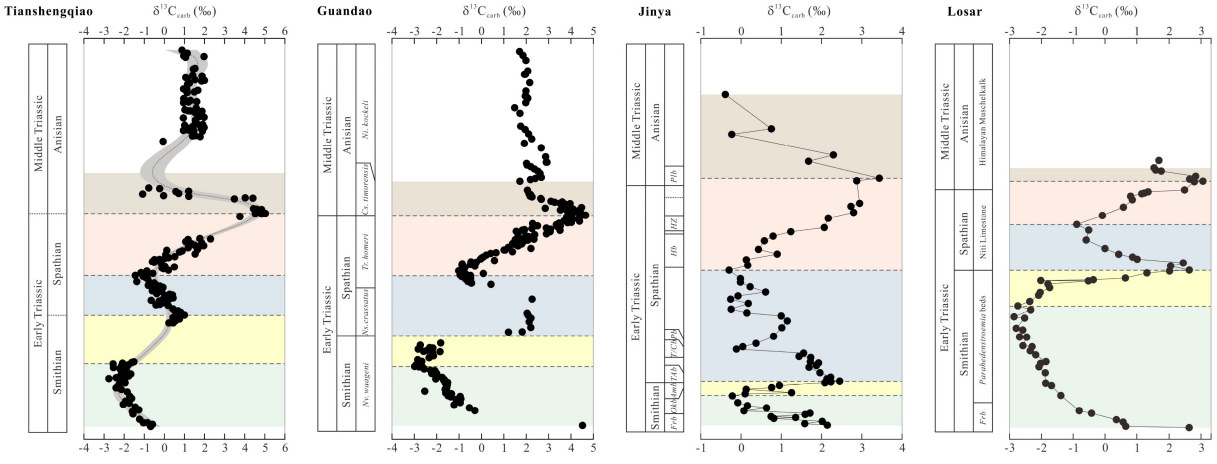

Figure 3. Comparison of the C-isotopic profiles of the Tianshengqiao (this study), Guandao[11], Jinya[14], and Losar[14] sections within the biostratigraphic framework. Abbreviations: *Frb* = *Flemingites rursiradiatus* beds, *Okb* = *Owenites koeneni* beds, *Amb* = *Anasibirites multiformis* beds, *TAb* = *Tirolitid n. gen. A.* beds, *T/Cb* = *Tirolites/Columbites* beds, *Pb* = *Procolumbites* beds, *Hb* = *Hellenites* beds, *HZ* = *Haugi* Zone, *Plb* = *Platycuccoceras* beds.

The negative $\delta^{13}C_{carb}$ excursion of 2.2‰ within the Member I of the Jialingjiang Formation can be correlated with the globally reported negative C-isotopic excursion that began at the early Smithian and reached a minimum value in the middle to late Smithian[11-15] (Figure 3). This negative C-isotopic shift represents one of the most significant C-isotopic excursions in the Early Triassic. The following positive $\delta^{13}C_{carb}$ excursion of 3.8‰ in the lower part of the Member III of the Jialingjiang Formation corresponds to the globally recognized positive C-isotopic excursion that began in the latest Smithian and peaked in the earliest Spathian[11-15] (Figure 3). After that, a negative $\delta^{13}C_{carb}$ excursion of 2.5‰ in the Member III of the Jialingjiang Formation can be correlated with the widely recognized negative C-isotopic excursion that began in the early Spathian and peaked in the middle Spathian[11-14] (Figure 3). The following positive $\delta^{13}C_{carb}$ excursion with a maximum of +5.0‰ at the base of the Member I of the Guanling Formation corresponds to the positive C-isotopic excursion that marks the Olenekian/Anisian boundary[11-15] (Figure 3). Above the maximum value, the $\delta^{13}C_{carb}$ profile in the Tianshengqiao section exhibits a third negative excursion, which can be correlated with the earliest Anisian negative C-isotopic excursion[11,14] (Figure 3). Finally, the $\delta^{13}C_{carb}$ values stabilize through the Member II of the Guanling Formation to the Yangliujing Formation, which is consistent with the C-isotopic stability in the Middle Triassic[11] (Figure 3).

Each of these $\delta^{13}C_{carb}$ excursions reported in the Tianshengqiao section is a unique event that can be correlated with those in the cotemporaneous sections globally. These C-isotopic events represent important chemostratigraphic markers that can be used to correlate the critical stratigraphic boundaries for the sections with inadequate biostratigraphic control. The similarity of the Early-Middle Triassic $\delta^{13}C_{carb}$ profile with those from other sections globally is indicative of the near completeness of the stratigraphic interval of the Tianshengqiao section. The $\delta^{13}C_{carb}$ excursions through the Early to Middle Triassic in the Tianshengqiao section correspond to the global perturbation of the C-isotopic compositions of seawater dissolved inorganic carbon (DIC).

5.3 Relationship of the carbon cycle perturbation to the prolonged biotic recovery

Multiple scenarios have been proposed to explain these C-isotopic fluctuations during the Early Triassic. For example, Payne and Kump[27] suggested that the Siberian Trap eruption provides a possible explanation for the repeated C-isotopic fluctuations. The negative C-isotope excursion during the Early Triassic was attributed to the release of isotopically depleted carbon during the Siberian Trap eruption[27]. The intervening positive C-isotope excursion was explained by increased productivity in response to the warming-induced anoxia and associated phosphate regeneration due to the Siberian Trap eruption[27]. However, the occurrence of sufficiently intense volcanism to affect the global biogeochemical cycle during the entire Early Triassic remains to be resolved[28]. Alternatively, Horacek et al.[12] suggested that episodic changes in the ocean's circulation may have caused the C-isotopic fluctuations during the Early Triassic. The positive C-isotopic excursion was attributed to ocean stratification[11]. The negative C-isotopic excursion was ascribed to the overturning of a previously stratified ocean, resulting in the release of isotopically depleted DIC from the deep waters[12]. However, the possible mechanism of overturning remains poorly understood. Sexton et al.[29] proposed that an anoxic ocean would have promoted the buildup of ^{13}C-depleted dissolved organic carbon in the deep waters. The development of oceanic anoxia during the Early Triassic has been documented from different paleolatitudes globally[5-8]. Moreover, many studies demonstrate that the Early Triassic oceans were dominated by microbes[30,31]. The widespread development of anoxia and the proliferation of microbes during the Early Triassic may have facilitated the buildup of a large ^{13}C-depleted dissolved organic carbon pool in the deep waters. Expansion of anoxic deep waters into the oxygenated upper water column due to environmental perturbations could have induced the oxidative decay of the organic carbon, resulting in the negative C-isotopic excursion[32,33]. In addition, high nutrient availability in the immediate aftermath of the

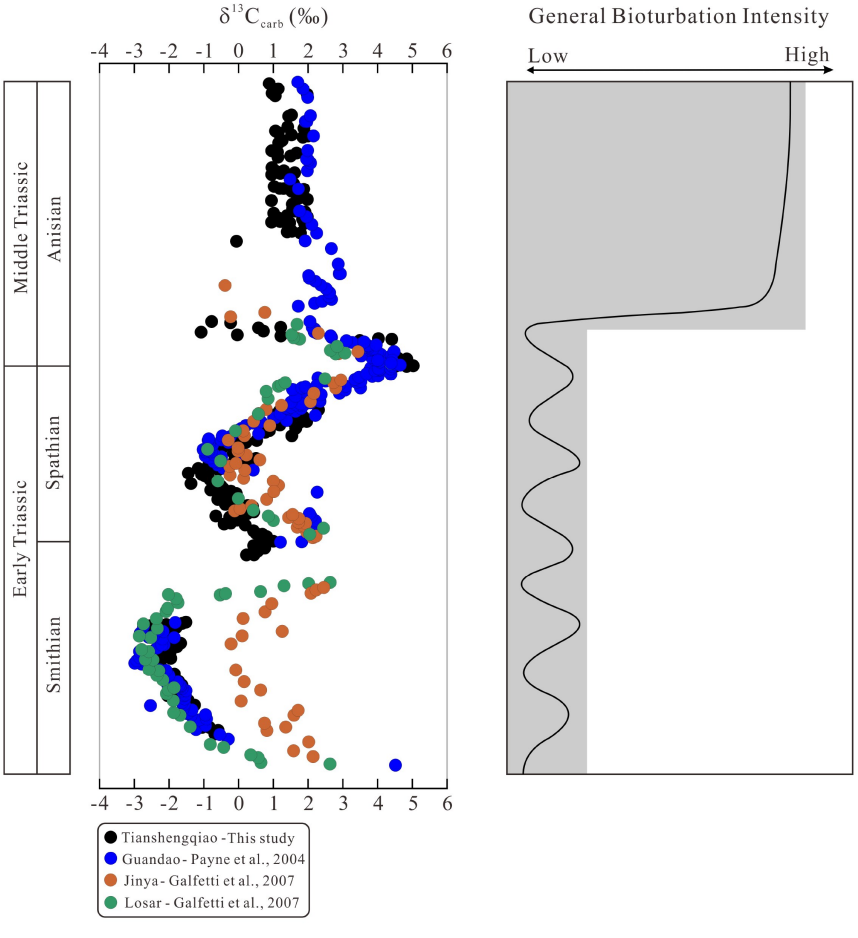

Figure 4. Composite C-isotopic curve and general bioturbation intensity during the Early-Middle Triassic. The C-isotopic data is from this study (Tianshengqiao) and three typical sections worldwide including Guandao[11], Jinya[14] and Losar[14]. The general bioturbation intensity is from Luo et al.[35].

expansion of anoxic deep waters could have enhanced primary productivity, generating the ensuing positive C-isotopic excursion[32,33]. These fluctuations of redox conditions may explain the repeated negative and positive C-isotopic excursions during the Early Triassic. This scenario is supported by the ocean redox studies which demonstrated the temporal coincidence between the negative C-isotopic excursion and the ocean anoxia[5,8]. Further paleo-redox studies carried out in the framework of chemostratigraphy worldwide can test this scenario and improve our understanding of the mechanistic links between the ocean chemistry changes and the Early Triassic C-isotopic excursions.

Previous studies have tested the relationship between the carbon cycle perturbation and the limited biotic recovery during the Early Triassic[11,13]. These studies based on the body fossil records suggested that the physical mechanisms of the C-isotopic fluctuations may have contributed to the prolonged Early Triassic biotic recovery[11,13]. Body fossil records provide several metrics of the biotic recovery process, revealing low global biodiversity and poorly functioning ecosystems dominated by nektonic organisms but devoid of benthic groups during the Early Triassic[11,13]. Trace fossils serve as alternative evidence for the delayed biotic recovery during the Early Triassic. Trace fossils potentially provide more detailed records of both epifaunal and infaunal organisms, and their preservation would not have been influenced by environmental changes, thus facilitating the assessment of the biotic recovery processes[18,34,35]. The ichnological studies in the Tianshengqiao section showed that the Lower Triassic is marked by low overall ichnodiversity, suggesting prolonged recovery and sustained harsh environmental conditions until the early Middle Triassic[18,34,35]. Our study reveals that large C-isotopic fluctuations characterize the Lower Triassic in the Tianshengqiao section. The stratigraphic coincidence between the C-isotopic fluctuations and the ichnologically observed interval of limited biotic recovery in the Tianshengqiao section corroborates the causal connection between carbon cycling and biological re-diversification following the Earth's most severe mass extinction (Figure 4).

6 Conclusions

A new high-resolution $\delta^{13}C_{carb}$ profile in the Tianshengqiao section permits recognition of well-established negative and positive excursions in the Early-Middle Triassic successions. Overall, the $\delta^{13}C_{carb}$ profile in the Tianshengqiao section can be comparable to those in the contemporaneous sections worldwide. The $\delta^{13}C_{carb}$ profile in the Tianshengqiao section shows a negative excursion of 2.2‰ within the Member I of the Jialingjiang Formation, succeeded by an increase of 3.8‰ in the lower part of the Member III of the Jialingjiang Formation. After that, $\delta^{13}C_{carb}$ displays a negative shift of 2.5‰ in the Member III of the Jialingjiang Formation, followed by an increase with a maximum of +5.0‰ at the base of the Member I of the Guanling Formation. Above the maximum value, the $\delta^{13}C_{carb}$ profile exhibits a third negative excursion and then recovers and stabilizes around +1‰ to +2‰ through the Member II of the Guanling Formation to the Yangliujing Formation. The new high-resolution $\delta^{13}C_{carb}$ record in the Tianshengqiao section provides additional evidence for the global instability of the Early Triassic carbon cycle. The stratigraphic coincidence between the C-isotopic fluctuations and the delayed biotic recovery has been documented in the Tianshengqiao section, suggesting a causal link between carbon cycle perturbation and prolonged biological recovery following the Earth's most severe mass extinction event.

Acknowledgments

This work is supported by the National Natural Science Foundation of China (41877319, 41703067, 41877318, 41772022), the USTC Research Funds of the Double First-Class Initiative (YD2080002005), and the Chinese Geological Survey (DD20190054).

Conflict of interest

The authors declare no conflict of interest.

Author information

ZHANG Guijie (corresponding author) is an associate research fellow at the University of Science and Technology of China (USTC). She received the PhD degree in geology from the USTC in 2016. Her research interests focus on the environmental change and its inter-relationship with biological evolution in Earth history. Her work combines field studies, stable isotope geochemistry, and mathematical modeling.

References

[1] Erwin D H. Extinction: How Life on Earth Nearly Ended 250 Million Years Ago. Princeton, NJ: Princeton University Press, 2006: 320.
[2] Knoll A H, Bambach R K, Payne J L, et al. Paleophysiology and end-Permian mass extinction. Earth and Planetary Science Letters, 2007, 256: 295-313.
[3] Chen Z Q, Benton M J. The timing and pattern of biotic recovery following the end-Permian mass extinction. Nature Geoscience, 2012, 5: 375-383.
[4] Sun Y D, Joachimski M M, Wignall P B, et al. Lethally hot temperatures during the Early Triassic greenhouse. Science, 2012, 338: 366-370.
[5] Grasby S E, Beauchamp B, Embry A, et al. Recurrent Early Triassic ocean anoxia. Geology, 2013, 41: 175-178.
[6] Huang Y G, Chen Z Q, Wignall P B, et al. Latest Permian

to Middle Triassic redox condition variations in ramp settings, South China: Pyrite framboid evidence. Geological Society of America Bulletin, 2017, 129 (1/2): 229-243.
[7] Zhang G J, Zhang X L, Hu D P, et al. Redox chemistry changes in the Panthalassic Ocean linked to the end-Permian mass extinction and delayed Early Triassic biotic recovery. Proceedings of the National Academy of Sciences of the United States of America, 2017, 114: 1806-1810.
[8] Zhang F F, Algeo T J, Cui Y, et al. Global-ocean redox variations across the Smithian-Spathian boundary linked to concurrent climatic and biotic changes. Earth-Science Reviews, 2019, 195: 147-168.
[9] Algeo T J, Twitchett R J. Anomalous Early Triassic sediment fluxes due to elevated weathering rates and their biological consequences. Geology, 2010, 38 (11): 1023-1026.
[10] Sun H, Xiao Y L, Gao Y J, et al. Rapid enhancement of chemical weathering recorded by extremely light seawater lithium isotopes at the Permian-Triassic boundary. Proceedings of the National Academy of Sciences of the United States of America, 2018, 115 (15): 3782-3787.
[11] Payne J L, Lehrmann D J, Wei J Y, et al. Large perturbations of the carbon cycle during recovery from the end-Permian extinction. Science, 2004, 305: 506-509.
[12] Horacek M, Richoz S, Brandner R, et al. Evidence for recurrent changes in Lower Triassic oceanic circulation of the Tethys: The $\delta^{13}C$ record from marine sections in Iran. Palaeogeography Palaeoclimatology Palaeoecology, 2007, 252: 355-369.
[13] Tong J N, Zuo J X, Chen Z Q. Early Triassic carbon isotope excursions from South China: Proxies for devastation and restoration of marine ecosystems following the end-Permian mass extinction. Geological Journal, 2007, 42: 371-389.
[14] Galfetti T, Bucher H, Brayard A, et al. Late Early Triassic climate change: Insights from carbonate carbon isotopes, sedimentary evolution and ammonoid paleobiogeography. Palaeogeography Palaeoclimatology Palaeoecology, 2007, 243: 394-411.
[15] Zhang L, Orchard M J, Algeo T J, et al. An intercalibrated Triassic conodont succession and carbonate carbon isotope profile, Kamura, Japan. Palaeogeography Palaeoclimatology Palaeoecology, 2019, 519: 65-83.
[16] Tong J N, Yin H F. The Lower Triassic of South China. Journal of Asian Earth Sciences, 2002, 20: 803-815.
[17] Zhao L S, Chen Y L, Chen Z Q, et al. Uppermost Permian to Lower Triassic conodont zonation from Three Gorges area, South China. Palaios, 2013, 28: 523-540.
[18] Luo M, George A D, Chen Z Q. Sedimentology and ichnology of two Lower Triassic sections in South China: Implications for the biotic recovery following the end-Permian mass extinction. Global and Planetary Change, 2016, 144: 198-212.
[19] Hu S X, Zhang Q Y, Chen Z Q, et al. The Luoping biota: Exceptional preservation, and new evidence on the Triassic recovery from end-Permian mass extinction. Proceedings of the Royal Society B, 2011, 278: 2274-2282.
[20] Benton M J, Zhang Q Y, Hu S X, et al. Exceptional vertebrate biotas from the Triassic of China, and the expansion of marine ecosystems after the Permo-Triassic mass extinction. Earth-Science Reviews, 2014, 137: 85-128.
[21] Kaufman A J, Knoll A H. Neoproterozoic variations in the C-isotopic composition of seawater: Stratigraphic and biogeochemical implications. Precambrian Research, 1995, 73: 27-49.
[22] Knauth L P, Kennedy M J. The late Precambrian greening of the Earth. Nature, 2009, 460: 728-732.
[23] Derry L A. A burial diagenesis origin for the Ediacaran Shuram-Wonoka carbon isotope anomaly. Earth and Planetary Science Letters, 2010, 294: 152-162.
[24] Swart P K. The geochemistry of carbonate diagenesis: The past, present, and future. Sedimentology, 2015, 62: 1233-1304.
[25] Higgins J A, Blattler C L, Lundstrom E A, et al. Mineralogy, early marine diagenesis, and the chemistry of shallow-water carbonate sediments. Geochimica et Cosmochimica Acta, 2018, 220: 512-534.
[26] Ahm A C, Bjerrum C J, Blattler C L, et al. Quantifying early marine diagenesis in shallow-water carbonate sediments. Geochimica et Cosmochimica Acta, 2018, 236: 140-159.
[27] Payne J L, Kump L R. Evidence for recurrent Early Triassic massive volcanism from quantitative interpretation of carbon isotope fluctuations. Earth and Planetary Science Letters, 2007, 256: 264-277.
[28] Hammer Ø, Jones M T, Schneebeli-Hermann E, et al. Are Early Triassic extinction events associated with mercury anomalies? A reassessment of the Smithian/Spathian boundary extinction. Earth-Science Reviews, 2019, 195: 179-190.
[29] Sexton P F, Norris R D, Wilson P A, et al. Eocene global warming events driven by ventilation of oceanic dissolved organic carbon. Nature, 2001, 471: 349-352.
[30] Chen Z Q, Wang Y B, Kershaw S, et al. Early Triassic stromatolites in a siliciclastic nearshore setting in northern Perth Basin, Western Australia: Geobiologic features and implications for post-extinction microbial proliferation. Global and Planetary Change, 2014, 121: 89-100.
[31] Fang Y H, Chen Z Q, Kershaw S, et al. An Early Triassic (Smithian) stromatolite associated with giant ooid banks from Lichuan (Hubei Province), South China: Environment and controls on its formation. Palaeogeography Palaeoclimatology Palaeoecology, 2017, 486: 108-122.
[32] Zhang G J, Zhang X L, Shen Y. Quantitative constraints on carbon cycling and temporal changes in episodic euxinia during the end-Permian mass extinction in South China. Chemical Geology, 2021, 562: 120036.
[33] Zhang G J, Zhang X L, Li D D, et al. Evidence for the expansion of anoxia during the Smithian from a quantitative interpretation of paired C-isotopes. Global and Planetary Change, 2021, 204: 103551.
[34] Feng X Q, Chen Z Q, Bottjer D J, et al. Additional records of ichnogenus *Rhizocorallium* from the Lower and Middle Triassic, South China: Implications for biotic recovery after the end-Permian mass extinction. Geological Society of America Bulletin, 2018, 130: 1197-1215.
[35] Luo M, Shi G R, Buatois L A, et al. Trace fossils as proxy for biotic recovery after the end-Permian mass extinction: A critical review. Earth-Science Reviews, 2020, 203: 103059.

早-中三叠世高分辨率的 $\delta^{13}C_{carb}$ 新记录：来自华南天生桥剖面的研究

张桂洁[1*]，张晓林[1]，周长勇[2]，黄金元[2]，张启跃[2]，胡世学[2]，文芠[2]，黄勰敏[1]

1. 中国科学技术大学地球和空间科学学院，安徽合肥 230026；
2. 中国地质调查局成都地质调查中心，四川成都 610081

* 通讯作者. E-mail：zhanggj@ustc.edu.cn

摘要：以往的研究发现早三叠世存在显著的碳循环扰动. 为了验证早-中三叠世碳同位素的变化趋势并深入理解这一时期碳循环规律，我们研究了华南天生桥剖面的早-中三叠世无机碳同位素（$\delta^{13}C_{carb}$）组成. 研究结果表明，天生桥剖面的 $\delta^{13}C_{carb}$ 值受到成岩作用的影响较小. $\delta^{13}C_{carb}$ 首先在嘉陵江组一段呈现幅度为 2.2‰的负偏移，随后在嘉陵江组三段底部呈现幅度为 3.8‰的正偏移. 接着，$\delta^{13}C_{carb}$ 在嘉陵江组三段出现幅度为 2.5‰的负偏移，随后在关岭组一段底部出现正偏移，最大值达到 5.0‰. 而后，$\delta^{13}C_{carb}$ 呈现第三次负偏移，并在关岭组二段至杨柳井组恢复且稳定在+1‰至+2‰左右. 天生桥剖面的 $\delta^{13}C_{carb}$ 地层变化趋势与全球同时期其他剖面的碳同位素地层演化趋势呈现出一致性. 这一特征表明天生桥剖面的早-中三叠世地层记录较为完整. 研究结果表明，天生桥剖面的 $\delta^{13}C_{carb}$ 变化特征能够代表全球碳循环的扰动. 此外，天生桥剖面记录的碳循环扰动与缓慢生命复苏之间具有地层一致性，这一特征表明碳循环扰动的物理机制可能是导致早三叠世缓慢生命复苏的主要原因.

关键词：化学地层对比；碳循环扰动；缓慢生命复苏；早-中三叠世